Bulletin of the Seismological Society of America, Vol. 99, No. 2B, pp. 1040–1049, May 2009, doi: 10.1785/0120080102

Tutorial on Surface Rotations from Wave Passage Effects: Stochastic Spectral Approach

by Zbigniew Zembaty

Abstract This article presents a concise review of the methods to obtain spectral densities of the rotational components of seismic ground motion from the spectral densities of both the translational components and wave propagation parameters. The rotational components are obtained by decomposing ground motion at the site into body and surface wave contributions with random amplitudes. To obtain rotation the resulting stochastic fields of body and surface waves are differentiated with respect to spatial coordinates. Assumption of plane waves radiating from a point source leads to two rotational components: rocking around a horizontal axis perpendicular to the source-site direction and torsion around a vertical axis. Construction of the rocking acceleration spectral density from *P*-, *SV*-, and Rayleigh-wave contributions as well as torsional spectral density from *SH* and Love waves (in terms of translational spectral densities and wave parameters) are discussed in detail. A short numerical analysis illustrates the proposed approach. A shift of the rotational spectra into higher frequencies compared to respective translational spectra is observed.

Introduction

The presence of the rotational components in seismic surface ground motion was occasionally discussed from the early period of seismic engineering (e.g., Immamura, 1937; Richter, 1958), and their engineering importance was pointed out as early as in the 1970s (Newmark and Rosenblueth, 1971; Flaga, 1979). Recent analyses give more and more arguments for treating seriously both the excitation surface rotations and rotations in structural seismic response (Jalali and Trifunac, 2009; Trifunac, 2009). However, without reliable direct measurements of the strong ground rotations, indirect methods of their assessment for engineering purposes shall be considered. Since the early 1980s two such groups of these methods have emerged in the literature:

- The first group of methods utilizes the synchronized measurements of translational ground motions at the short distances (e.g., Niazi, 1986; Oliveira and Bolt, 1989; Castellani and Zembaty, 1996).
- The second group of methods is based on the analyses of the wave passage effects at the site, constructing respective wave field, and on differentiating it with respect to a spatial coordinate. These methods began from the landmark article by Trifunac (1982) and were later developed by Lee and Trifunac (1985, 1987, 2009), Rutenberg and Heidebrecht (1985), Castellani and Boffi (1989), Zembaty *et al.* (1993), and Li *et al.* (1997, 2002).

In what follows, the idea of body and surface-waves decompositions (Trifunac, 1982; Zembaty *et al.*, 1993; Li *et al.*, 2002) will be revisited to formulate algorithms for constructing spectral densities of the rocking and torsional components in terms of the translational spectra, their cospectra, and wave parameters.

Statement of the Problem

Theoretically, any site on the ground surface can be subjected to six motions during an earthquake:

- three translations $u(t)$, $v(t)$, and $w(t)$ along x, y, and z axes and
- three rotations around these axes $\psi_x(t)$, $\psi_y(t)$, and $\psi_z(t)$.

The rotation $\psi_z(t)$ around a vertical axis is usually called torsion and will be denoted here as $\varphi(t)$, while the rotations $\psi_x(t)$ and $\psi_y(t)$ around horizontal axes are called rockings. Directing the axis x toward the epicenter defines the system of so-called principal axes. Penzien and Watabe (1975) have shown that three translational components of seismic ground motion along the respective principal axes x, y, and z are uncorrelated. What is more, when spatial seismic effects at two distinct surface points A and B are analyzed, the respective coherence matrix transforms as a tensor when the system of coordinates is changed (e.g., Zembaty, 1997). As it will be shown later, the decomposition of plane waves analyzed in the coordinate system of principal axes leads only to two rotations:

- torsion $\varphi = \psi_z$ around a vertical axis and

- rocking $\psi = \psi_y$ around a horizontal axis y, perpendicular to site-epicenter direction (x axis).

Consider now elastic and isotropic half-space (Fig. 1). In this article only the two rotations (φ and ψ) previously defined are considered and drawn in Figure 1. The seismic signal comes to the site from beneath in the form of body waves and horizontally on the surface as surface waves. To obtain rotation each of these effects shall be treated separately. The rotations from body waves were first examined by Trifunac (1982), while the Rayleigh and Love waves were first examined by Zembaty *et al.* (1993) and Li *et al.* (2002). Before any analysis of the rotational effects, each type of these waves shall now be examined with respect to the decoupled spatial effects on the ground surface.

Body-Wave Decomposition at the Ground Surface

P-Wave Effects

Consider P waves incident on the ground surface (Fig. 2). Each incident P wave generates a reflected P wave going down under the same angle $\Theta_{PP} = \Theta_P$ and a reflected SV wave at an angle Θ_{PS}, which results from the familiar formula of the geometric optics (e.g., Achenbach, 1973 or Aki and Richards, 2002)

$$\sin(\Theta_P)/\sin(\Theta_{PS}) = c_P/c_S = S, \tag{1}$$

where c_P and c_S are the P- and S-wave velocities of propagation. Taking into account other laws of geometrical optics, it is possible to obtain amplitudes of horizontal (A_x) and vertical (A_z) motions contributed by the P waves,

$$A_x = U_P A_P \tag{2}$$

and

$$A_z = W_P A_P, \tag{3}$$

in terms of the amplitudes A_P of the P waves, where coefficients U_P and W_P are formulated when observing the summations of respective projections of the motions on the free surface (Fig. 2),

$$U_P = (1 + P_P)\sin\Theta_P + P_P \cos\Theta_{PS} \tag{4}$$

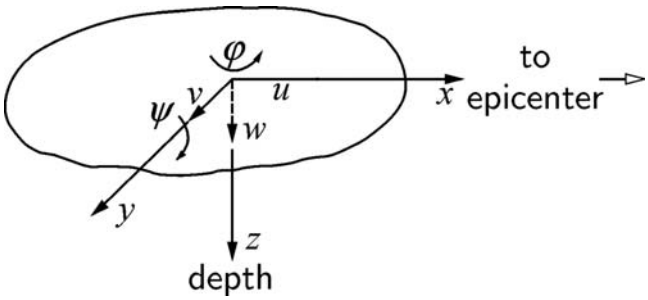

Figure 1. Principal axes and two rotations on the ground surface.

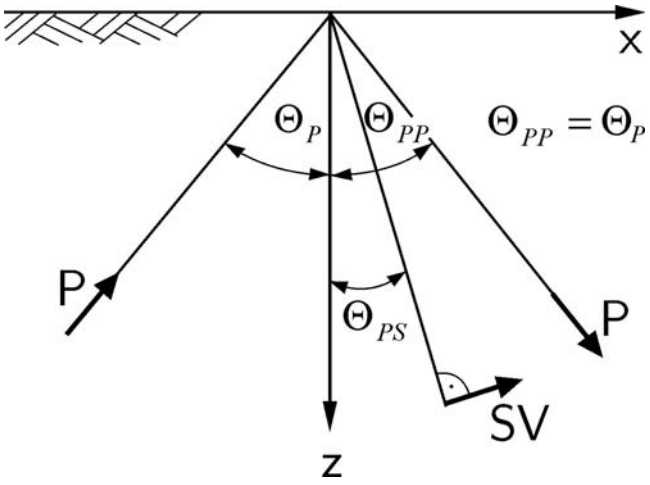

Figure 2. P waves incident on the ground surface.

and

$$W_P = (P_P - 1)\cos\Theta_P + P_S \sin\Theta_{PS}. \tag{5}$$

The reflection coefficients P_P and P_S of P waves from the free surface are given by the following formulas (Achenbach, 1973; Aki and Richards, 2002):

$$P_P = \frac{-(\frac{1}{c_S^2} - 2p^2) + 4p^2 \frac{\cos(\Theta_P)}{c_P}\frac{\cos(\Theta_{PS})}{c_S}}{(\frac{1}{c_S^2} - 2p^2)^2 + 4p^2 \frac{\cos(\Theta_P)}{c_P}\frac{\cos(\Theta_{PS})}{c_S}}, \tag{6}$$

$$P_S = \frac{4\frac{c_P}{c_S} p \frac{\cos(\Theta_P)}{c_P}(\frac{1}{c_S^2} - 2p^2)}{(\frac{1}{c_S^2} - 2p^2)^2 + 4p^2 \frac{\cos(\Theta_P)}{c_P}\frac{\cos(\Theta_{PS})}{c_S}}, \tag{7}$$

where $p = \sin(\Theta_P)/c_P$ is the horizontal slowness of the incident P waves.

SV-Wave Effects

Now consider the SV waves incident on the ground surface at the angle Θ_{SV} (Fig. 3). In this case the reflection from

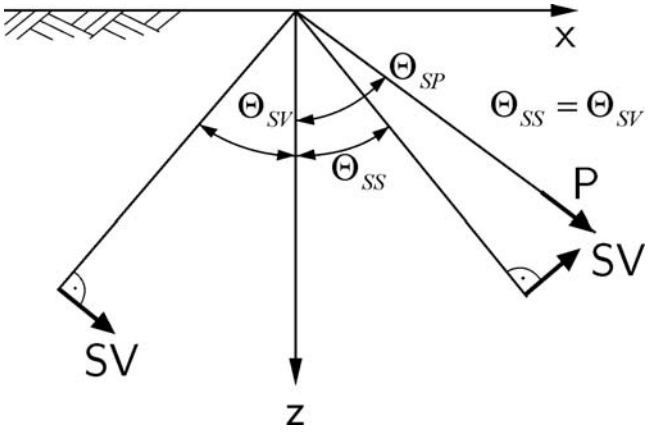

Figure 3. SV waves incident on the ground surface.

the free surface results in an *SV* wave reflected at the same angle $\Theta_{SS} = \Theta_{SV}$ as well as a *P* wave reflected at the angle Θ_{SP}:

$$\sin(\Theta_{SV})/\sin(\Theta_{SP}) = c_S/c_P. \tag{8}$$

Analogously to equations (2) and (3) the amplitudes of respective horizontal (A_x) and vertical (A_z) contributions from the *SV* waves can be written in terms of the amplitudes A_{SV} of the *SV* waves

$$A_x = U_S A_{SV} \tag{9}$$

and

$$A_z = W_S A_{SV}, \tag{10}$$

where U_S and W_S are formulated by observing the summations of respective projections of the motions induced by *SV* waves at the free surface (Fig. 3):

$$U_S = (1 + S_S)\cos(\Theta_{SV}) + S_P \sin(\Theta_{SP}) \tag{11}$$

and

$$W_S = (1 - S_S)\sin(\Theta_{SV}) - S_P \cos(\Theta_{SP}). \tag{12}$$

The reflection coefficients S_P and S_S of *SV* waves from the free surface are equal to

$$S_P = \frac{4\frac{c_S}{c_P} p \frac{\cos(\Theta_{SV})}{c_S}\left(\frac{1}{c_S^2} - 2p^2\right)}{\left(\frac{1}{c_S^2} - 2p^2\right)^2 + 4p^2 \frac{\cos(\Theta_{sp})}{c_P}\frac{\cos(\Theta_{SV})}{c_S}}, \tag{13}$$

$$S_S = \frac{\left(\frac{1}{c_S^2} - 2p^2\right)^2 - 4p^2 \frac{\cos(\Theta_{SP})}{c_P}\frac{\cos(\Theta_{SV})}{c_S}}{\left(\frac{1}{c_S^2} - 2p^2\right)^2 + 4p^2 \frac{\cos(\Theta_{SP})}{c_P}\frac{\cos(\Theta_{SV})}{c_S}}, \tag{14}$$

where $p = \sin(\Theta_{SV})/c_S$ now represents the horizontal slowness of incident *SV* waves.

SH-Wave Effects

Consider now the *SH* waves incident at the free surface with angle Θ_{SH} (Fig. 4). This wave is reflected at the same angle, and the same amplitude is kept for the reflected wave; thus, the amplitudes of the ground motions along axes *x* and *z* are equal to zero, while the amplitude along axis *y* does not depend on the angle of incidence and equals

$$A_v = 2A_{SH}. \tag{15}$$

Surface Wave Decomposition at the Ground Surface

Rayleigh Waves

The vertical and horizontal components of Rayleigh waves propagating at the surface in plane *x*, *z* with amplitude

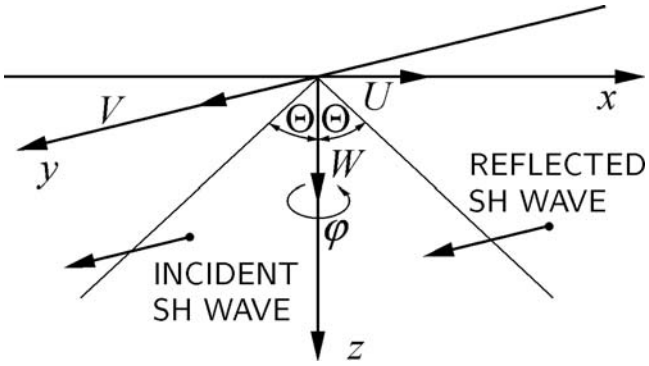

Figure 4. *SH* waves incident on the ground surface.

A_R can be written directly in the form of the following spatial field:

$$w_R(t) = A_R \exp\left[i\omega\left(t - \frac{x}{c_R}\right)\right], \tag{16}$$

$$u_R(t) = A_R \exp\left[i\omega\left(t - \frac{x}{c_R}\right)\right], \tag{17}$$

where c_R stands for Rayleigh-wave velocity of propagation.

Love Waves

Love waves propagate along axis *x* when there is a low-velocity top layer above the elastic half-space. These waves generate displacements $v(t)$ along the *y* axis (Fig. 1), which are perpendicular to the direction of propagation, with the remaining two orthogonal displacements kept zero ($u = w = 0$). Thus, the Love wave with amplitude A_L can be written as follows:

$$v_L(t) = A_L \exp\left[i\omega\left(t - \frac{x}{c_L}\right)\right], \tag{18}$$

where c_L represents velocity of propagation of the Love waves.

Calculating Rotations from Respective Wave Contributions

According to the basic formulae of the continuum mechanics, the rocking component (about the *y* axis) depends on the vertical spatial field of seismic ground motion

$$\psi = \frac{\partial w}{\partial x}, \tag{19}$$

while the respective torsion (about the *z* axis) depends on two orthogonal horizontal components

$$\varphi = \frac{1}{2}\left(\frac{\partial v}{\partial x} - \frac{\partial u}{\partial y}\right). \tag{20}$$

Now the rotational effects resulting from any type of the waves described earlier can be obtained in two steps:

(1) by constructing spatial seismic fields induced by respective waves at the free surface, and
(2) by differentiating these fields with respect to spatial coordinates (equations 19 and 20).

It should be noted here that the realistic ground motion is a composition of various wave effects including, in particular,

- various angles of incidence and
- various velocities of propagation.

The first effect is derived from the fact that the ground beneath the site is often composed of layers, which will affect the respective body-wave rays. The appropriate angles and velocities of body waves at the ground surface can be calculated using well known Haskell–Thomson formulae (Thomson, 1950; Haskell, 1953), which is a rather tedious but straightforward procedure. The second effect is perhaps more difficult to account for, as the velocities of waves will depend on the frequencies of respective harmonics and tend to form groups.

Finally, one has to decide about the contribution of various wave types, particularly the presence of the surface waves. This means that the realistic prediction of the rotational components from the wave passage effects contains many unknown or random elements, and it may be difficult to make it reliable. Thus, the researchers usually assume various simplifications (see Lee and Trifunac, 1985, 1987; Zembaty *et al.*, 1993; Li *et al.*, 1997, 2002; Lee and Trifunac, 2009). As it was pointed out by Lee and Trifunac in their very recent article, even when including all of the effects discussed here in the properly synthesized rotational ground motion, many other complicated phenomena affecting rotational ground motion are still not covered (e.g., nonlinear site response). That is why any ground-motion models based on linear theory and numerical models shall be treated very cautiously (Lee and Trifunac, 2009).

In what follows the procedure to obtain a spectral representation of the rocking component based on the spectral densities of the translational components will be given in detail following Zembaty *et al.* (1993).

Composing Spectral Density of the Rocking Ground Motion Based on Translational Spectral Densities

The previous sections lead to the conclusion that the rocking component will be an effect of (body) *P* and *SV* waves as well as (surface) Rayleigh waves. First consider the effect of body waves.

Rocking from Body-Wave Decomposition

Assume now that the horizontal and vertical accelerations along the x and z axes (Fig. 1) can be written as infinitesimal contributions of stochastic processes written in form of the integrands of Stieltjes–Fourier integrals (see the Appendix)

$$e^{i\omega\tau} d\hat{\ddot{u}}(\omega), \qquad e^{i\omega\tau} d\hat{\ddot{w}}(\omega) \tag{21}$$

in frequency band interval $(\omega,\ \omega + d\omega)$. The motion corresponding to this interval can be written as the sum of *P*- and *SV*-wave contributions

$$d\ddot{u} = d\ddot{u}_P + d\ddot{u}_S, \qquad d\ddot{w} = d\ddot{w}_P + d\ddot{w}_S. \tag{22}$$

Substituting the spectral representations (21) for $\ddot{u}$ and $\ddot{w}$ in (22) one obtains

$$\begin{aligned} e^{i\omega\tau} d\hat{\ddot{u}}(\omega) &= U_P e^{i\omega\tau} d\hat{\ddot{\Phi}}_P(\omega) + U_S e^{i\omega\tau} d\hat{\ddot{\Phi}}_S(\omega), \\ e^{i\omega\tau} d\hat{\ddot{w}}(\omega) &= W_P e^{i\omega\tau} d\hat{\ddot{\Phi}}_P(\omega) + W_S e^{i\omega\tau} d\hat{\ddot{\Phi}}_S(\omega), \end{aligned} \tag{23}$$

where $\hat{\ddot{\Phi}}_P(\omega)$, $\hat{\ddot{\Phi}}_S(\omega)$ are the random functions with orthogonal increments (equations A1–A3), and U_P, U_S, W_P, and W_S are the coefficients given by the equations (4), (5), (11), and (12). It should be pointed out that for the simplicity of this analysis, we assume here that both *P* and *SV* waves come to the surface at the same angle $\Theta = \Theta_P = \Theta_{SV}$, which effectively means the assumption of the homogeneous half-space beneath the site. Solving the system of equation (23) for the *P*- and *SV*-wave contributions, one obtains the inverse of equation (23):

$$\begin{aligned} e^{i\omega t} d\hat{\ddot{\Phi}}_P(\omega) &= \frac{W_S}{D} e^{i\omega t} d\hat{\ddot{u}}(\omega) - \frac{U_S}{D} e^{i\omega t} d\hat{\ddot{w}}(\omega), \\ e^{i\omega t} d\hat{\ddot{\Phi}}_S(\omega) &= \frac{U_P}{D} e^{i\omega t} d\hat{\ddot{w}}(\omega) - \frac{W_S}{D} e^{i\omega t} d\hat{\ddot{u}}(\omega), \end{aligned} \tag{24}$$

where $D = U_P W_S - W_P U_S$. Thus, the vertical motion can be presented as the sum of two wave terms propagating in the x direction with different velocities as follows:

$$\begin{aligned} d\ddot{w}(t,\omega,x) = {} & W_P \exp\left\{ i\omega\left[t - \frac{x\sin(\Theta)}{c_P} \right] \right\} d\hat{\ddot{\Phi}}_P(\omega) \\ & + W_S \exp\left\{ i\omega\left[t - \frac{x\sin(\Theta)}{c_S} \right] \right\} d\hat{\ddot{\Phi}}_S(\omega). \end{aligned} \tag{25}$$

The incremental rocking acceleration equals then

$$d\ddot{\psi}(t,\omega) = \frac{\partial}{\partial x} d\ddot{w}(t,\omega,x)\bigg|_{x=0}, \tag{26}$$

$$d\ddot{\psi}(t,\omega,x) = W_P\left[-i\omega\frac{\sin(\Theta)}{c_P}\right] \times \exp\left\{i\omega\left[t-\frac{x\sin(\Theta)}{c_P}\right]\right\} d\hat{\hat{\Phi}}_P(\omega) + W_S\left[-i\omega\frac{\sin(\Theta)}{c_S}\right] \times \exp\left\{i\omega\left[t-\frac{x\sin(\Theta)}{c_S}\right]\right\} d\hat{\hat{\Phi}}_S(\omega). \quad (27)$$

Substituting $x = 0$ and taking into account equation (24) one obtains

$$d\ddot{\psi}(t,\omega) = W_P\left[-i\omega\frac{\sin(\Theta)}{c_P}\right]e^{i\omega t}\frac{W_S}{D}d\hat{\ddot{u}}(\omega) - W_P\left[-i\omega\frac{\sin(\Theta)}{c_P}\right]e^{i\omega t}\frac{U_s}{D}d\hat{\ddot{w}}(\omega) + W_S\left[-i\omega\frac{\sin(\Theta)}{c_P}\right]e^{i\omega t}\frac{U_p}{D}d\hat{\ddot{w}}(\omega) - W_S\left[-i\omega\frac{\sin(\Theta)}{c_S}\right]e^{i\omega t}\frac{W_P}{D}d\hat{\ddot{u}}(\omega). \quad (28)$$

Introducing new coefficients

$$W_x = \frac{W_P W_S}{D}\frac{\sin(\Theta)}{c_P} - \frac{W_P W_S}{D}\frac{\sin(\Theta)}{c_S}, \qquad W_z = \frac{U_P W_S}{D}\frac{\sin(\Theta)}{c_S} - \frac{W_P U_S}{D}\frac{\sin(\Theta)}{c_P} \quad (29)$$

results in

$$d\ddot{\psi}(t,\omega) = W_x(-i\omega)e^{i\omega t}d\hat{\ddot{u}}(\omega) + W_z(-i\omega)e^{i\omega t}d\hat{\ddot{w}}(\omega). \quad (30)$$

Finally, after integrating in the whole frequency domain one obtains the spectral decomposition of the rocking component

$$\ddot{\psi}(t) = \int_{-\infty}^{\infty} W_x(-i\omega)e^{i\omega t}\,d\hat{\ddot{u}}(\omega) + \int_{-\infty}^{\infty} W_z(-i\omega)e^{i\omega t}\,d\hat{\ddot{w}}(\omega), \quad (31)$$

which by applying equations (A2) and (A3) from the Appendix, can easily be used to obtain any stochastic characteristics of ψ (e.g., a correlation function, power spectral density). For example, the mean square rocking acceleration is given by

$$\sigma^2_{\ddot{\psi}} = \int_{-\infty}^{\infty}|W_x|^2\omega^2 S_{\ddot{u}}(\omega)d\omega + 2\int_{-\infty}^{\infty} W_x W_z^*\omega^2 S_{\ddot{u}\,\ddot{w}}(\omega)\,d\omega + \int_{-\infty}^{\infty}|W_z|^2\omega^2 S_{\ddot{w}}(\omega)\,d\omega, \quad (32)$$

where the asterisk denotes a complex conjugate. The integrand in equation (32) is the power spectral density of the rocking component:

$$S_{\ddot{\psi}}(\omega) = |W_x|^2\omega^2 S_{\ddot{u}}(\omega) + 2W_x W_z^* S_{\ddot{u}\,\ddot{w}}(\omega) + |W_z|^2\omega^2 S_{\ddot{w}}(\omega). \quad (33)$$

It can be seen from the derived formulae that the rotational spectrum is a function of the first derivatives of the vertical and horizontal accelerations (the ω^2 multiplier). In other words, the function of the third derivative of respective displacements as $S_{\dddot{u}}(\omega) = \omega^6 S_u(\omega)$. It should also be noted that if one follows the Penzien and Watabe (1975) assumption, the second term of equation (33) vanishes, as there is no correlation between vertical and horizontal components. In this case equation (33) can be further simplified when assuming the same spectral density for both horizontal and vertical ground motions differing only by an intensity factor η, that is

$$S_{\ddot{w}}(\omega) = \eta^2 S_{\ddot{u}}(\omega). \quad (34)$$

This leads to

$$S_{\ddot{\psi}}(\omega) = (|W_x|^2 + \eta^2|W_z|^2)\omega^2 S_{\ddot{u}}(\omega). \quad (35)$$

The value of η can be estimated from the statistical analyses of earthquake records. For example, following Trifunac and Brady (1975) it can be taken approximately as 0.5. On the other hand, in the near field the vertical component can be as intensive as the horizontal one (e.g., the 1995 Northridge earthquake). In any case the contribution of vertical and horizontal components to the total rocking is controlled by the values of the coefficients W_x and W_z.

In Figure 5a and b the moduli of these two coefficients are presented as functions of the incidence angle of body waves, the same for both P and SV waves $\Theta_P = \Theta_{SV}$. The plots are calculated for three sets of data given in Table 1 and representing firm (stiff) ground and hard rocks. Each set of data results in different critical angles. The values of these angles are displayed as straight lines in Figure 5.

For $\Theta < \Theta_{cr}$, W_x is real and negative while W_z is also real but positive, although in any case the signs are lost when formulating the spectral density. It can be seen from Figure 5 that W_x and W_z increase for an overcritical angle with a considerable variation with respect to the values of Poisson's ratio ν for W_x and with little variation for W_z. It means that the rocking component increases with increasing incidence angle, and that the vertical excitations contribute more to the rocking than the horizontal ones. The horizontal contribution to the rocking is, however, more sensitive to the choice of ground and wave parameters, particularly for overcritical incidence angles.

In Figure 6a the coefficient of equation (35) (i.e., $|W_x|^2 + \eta^2|W_z|^2$) is shown for three values of ν versus incidence angle Θ. It is a key coefficient in an analysis of rotations, because together with the multiplier ω^2 this coefficient transforms translation spectral density into rocking spectral density.

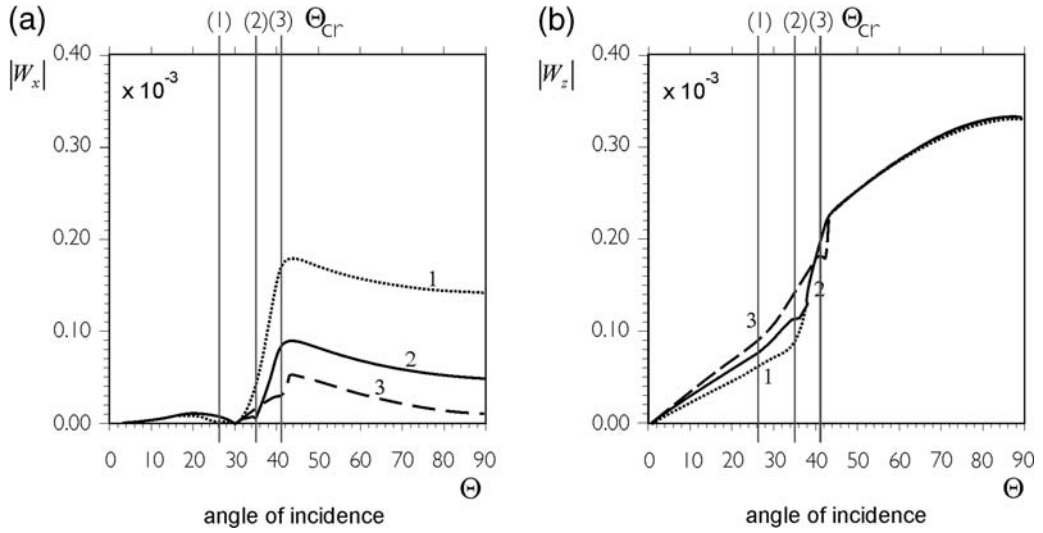

Figure 5. Moduli of W_x and W_y coefficients (equation 29) versus incidence angle Θ calculated for three values of Poisson coefficient (1) $\nu = 0.38$, (2) $\nu = 0.25$, and (3) $\nu = 0.10$.

To investigate the contribution of possible cross correlation of horizontal and vertical components one may also assume an unlikely extreme case of full (100%) horizontal–vertical correlation. In this case equation (33) takes the following form:

$$S_{\ddot{\psi}}(\omega) = (|W_x|^2 + 2\eta W_x W_z^* + \eta^2 |W_z|^2)\omega^2 S_{\ddot{w}}(\omega). \quad (36)$$

The multiplier of equation (36) (i.e., $|W_x|^2 + 2\eta W_x W_z^* + \eta^2|W_z|^2$) is plotted in Figure 6b. It can be seen that Poisson's ratio influences the rocking response substantially. The difference for $\nu = 0.38$ and $\nu = 0.25$ is particularly substantial. It can also be seen that cross correlation between vertical and horizontal components may increase the rocking ground motion up to about 30%. All plots in Figure 6a and b show dramatic increase in the rocking component for overcritical incidence angles. In Figure 6c and d the effect of the vertical-to-horizontal intensity factor η on the rocking component coefficients without horizontal–vertical correlation ($|W_x|^2 + \eta^2|W_z|^2$) and with full correlation ($|W_x|^2 + 2\eta W_x W_z^* + \eta^2|W_z|^2$) are analyzed. The plots are calculated for three values of $\eta = 0.25$, $\eta = 0.5$, and $\eta = 2.0$. As could be expected the η factor substantially affects the rocking component, while the difference between lack of horizontal–vertical correlation (Fig. 6c) and full correlation (Fig. 6d) plays a less important role.

Table 1
Data for Numerical Calculations

c_P (m/sec)	6800	5200	4500
c_S (m/sec)	3000	3000	3000
$S = c_P/c_S$	2.27	1.73	1.50
Poisson Modulus ν	0.38	0.25	0.10
Θ_{cr} (deg)	26.14	35.26	41.81

Rocking from Rayleigh Waves

A quantitative estimation of the contribution of surface waves (and in particular the Rayleigh waves) to the total ground motion is not an easy task. Identification of the wave types for the strong events at a particular site becomes possible via a dispersion analysis, when large scale measurements of ground motion are carried out as in the spatial measurements of the Strong-Motion Accelerograph Array in Taiwan, Phase 1 (SMART-1) network. A rough and simple idea has been proposed by Sugito *et al.* (1984). Analyzing some Japanese strong-motion records, they proposed to separate surface waves from the total ground motion by using the criterion of the first arrival time t_S and a bandlimit ω_S. Following their approach, the motion due to surface waves should be subtracted from the total motion and treated separately (Fig. 7).

When considering the rocking component we restrict our attention to Rayleigh waves. In an analogy to the earlier treatment, the acceleration due to surface waves in the frequency range $\omega, \omega + d\omega$ can be written in the form of a wave propagating in the horizontal direction with the velocity of Rayleigh waves c_R

$$d\ddot{w}_R = \exp\left[i\omega\left(t - \frac{x}{c_R}\right)\right] d\hat{\ddot{w}}(\omega). \quad (37)$$

From equation (37) the incremental surface rocking can be obtained

$$d\ddot{\psi}_R = \frac{\partial}{\partial x} d\ddot{w}_R(t, \omega, x)\bigg|_{x=0} = \left(-\frac{i\omega}{c_R}\right) e^{i\omega t} d\hat{\ddot{w}}(\omega). \quad (38)$$

Taking into account the previously listed criteria of wave separation ($t > t_S$, $-\omega_S < \omega < \omega_S$) one obtains

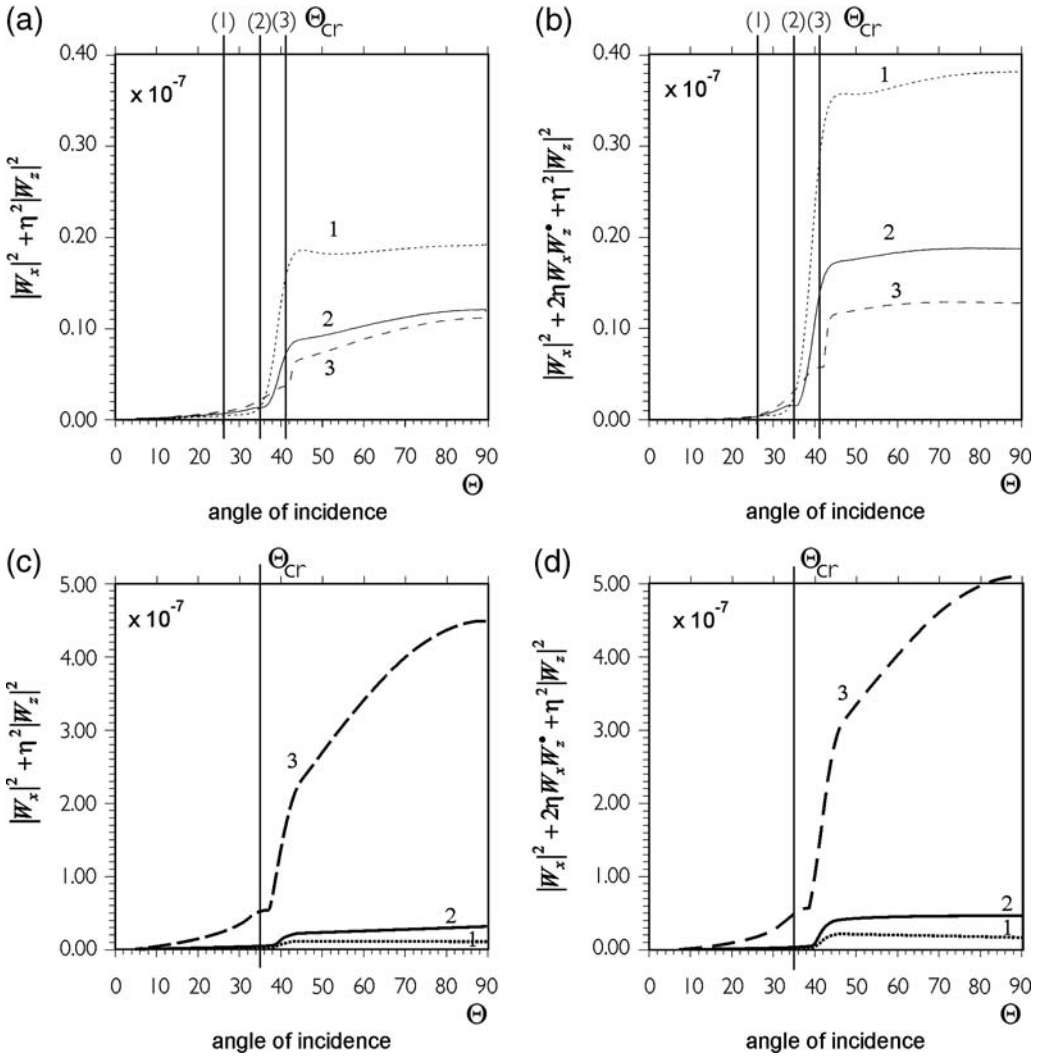

Figure 6. The coefficients of rocking spectral densities with (a) and (c) zero horizontal–vertical correlation and with (b) and (d) full correlation shown for (a) and (b) three values of Poisson coefficient (1) $\nu = 0.38$, (2) $\nu = 0.25$, and (3) $\nu = 0.10$ and three values of vertical-to-horizontal coefficient (1) $\eta = 0.25$, (2) $\eta = 0.5$, and (3) $\eta = 2.0$ with $\nu = 0.25$.

$$d\ddot{\psi}_R = \left(-\frac{i\omega}{c_R}\right) e^{i\omega t} d\hat{\ddot{w}}(\omega) \quad \text{for} \quad -\omega_S < \omega < \omega_S \quad \text{and} \quad t > t_S, \tag{39}$$

$$\ddot{\psi}_R = \int_{-\omega_s}^{\omega_s} W_R(-i\omega) e^{i\omega t}\, d\hat{\dot{w}}(\omega) \quad \text{for} \quad t > t_S, \tag{40}$$

where $W_R = 1/c_R$. From this equation and equations (A2) and (A3), one may write the equation for spectral density of the rocking acceleration contributed by the surface waves

$$S_{\ddot{\psi}}(t,\omega) = W_R^2 \omega^2 S_{\dot{w}}(t,\omega) \quad \text{for} \quad -\omega_S < \omega < \omega_S \quad \text{and} \quad t > t_S. \tag{41}$$

This formula only roughly shows the dependence between vertical and rotational spectral density from Rayleigh-wave propagation. The analysis of joint effects of body and surface waves should be done in both the time and frequency domain. This general approach, including the nonstationary, evolutionary description of stochastic processes, is presented in detail in the article by Zembaty *et al.* (1993).

Spectral Density of the Torsional Ground Motion Based on Translational Spectral Densities

Torsion from Body Waves

From equation (20) it is evident that the torsional component (ground rotations around a vertical axis) will be built by the derivatives of two horizontal motions $u(t)$ and $v(t)$. For plane waves and the principal coordinate system from Figure 1, the *SH* component along the y axis depends only on coordinate x, while *P* and *SV* contributions (along the x axis) do not depend on y; therefore, equation (20) gives

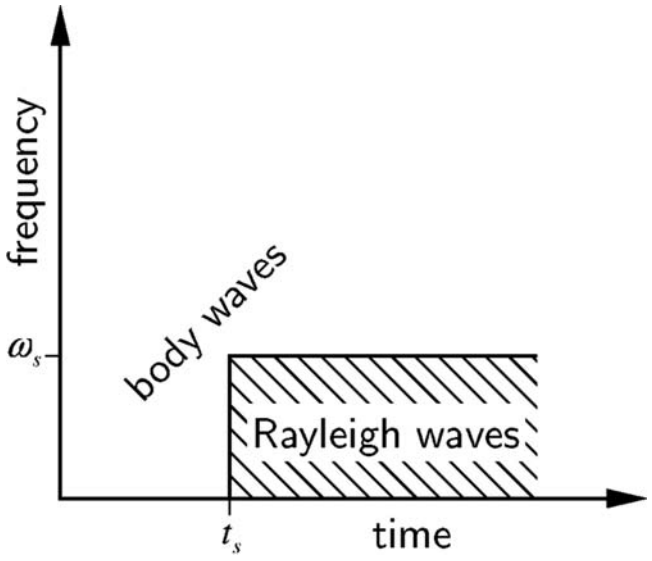

Figure 7. Body- and surface-wave separation is shown.

$$\varphi = \frac{1}{2}\left(\frac{\partial v}{\partial x} - \frac{\partial u}{\partial y}\right) = \frac{1}{2}\frac{\partial v}{\partial x}. \tag{42}$$

Introducing the random, incremental *SH*-wave contribution to the acceleration along the y axis (Fig. 4)

$$d\ddot{v} = 2\exp\left\{i\omega\left[t - \frac{x\sin(\Theta_{SH})}{c_S}\right]\right\} d\hat{\ddot{\Phi}}_{SH}(\omega), \tag{43}$$

which for $x = 0$ equals

$$d\ddot{v} = 2e^{i\omega t} d\hat{\ddot{\Phi}}_{SH}(\omega), \tag{44}$$

one obtains the incremental torsion in an analogous way (as in the previous section on rocking from body-wave decomposition):

$$d\ddot{\varphi} = \frac{1}{2}\frac{\partial}{\partial x} d\ddot{v}(t,\omega,x)\bigg|_{x=0} = -i\omega\frac{\sin(\Theta_{SH})}{c_S} \times e^{i\omega t} d\hat{\ddot{\Phi}}_{SH}(\omega). \tag{45}$$

Taking into account equation (44) gives

$$d\ddot{\varphi} = -\frac{i\omega}{2}\frac{\sin(\Theta_{SH})}{c_S} d\hat{\ddot{v}}(\omega). \tag{46}$$

Following further the procedure of the previous section on rocking from body-wave decomposition and taking into account equations (A1) to (A3), it is possible to formulate spectral density of torsional accelerations in terms of spectral density of horizontal accelerations $\ddot{v}(t)$:

$$S_{\ddot{\varphi}}(\omega) = \frac{\sin^2(\Theta_{SH})}{(2c_S)^2}\omega^2 S_{\ddot{v}}(\omega). \tag{47}$$

In Figure 8 the coefficient $\sin^2(\Theta_{SH})/(2c_S)^2$ from equation (47) is plotted versus angle of incidence Θ_{SH}. It can be seen that the torsional component increases with the increasing angle of incidence.

Torsion from Love Waves

The nonzero component of Love waves appears along the y axis, transversal to its propagation direction (along the x axis). Respective torsional acceleration can be obtained in an analogous way as it was done for Rayleigh waves. Random incremental horizontal accelerations due to Love waves can be written as

$$d\ddot{v}_L = \exp\left[i\omega\left(t - \frac{x}{c_L}\right)\right] d\hat{\ddot{v}}_L(\omega) \tag{48}$$

from which the torsional, incremetal accelerations equal

$$d\ddot{\varphi}_L = \frac{1}{2}\frac{\partial}{\partial x} d\ddot{v}_L(t,\omega,x)\bigg|_{x=0} = \left(-\frac{i\omega}{2c_L}\right) e^{i\omega t} d\hat{\ddot{v}}_L(\omega). \tag{49}$$

Integrating in the whole frequency domain one obtains respective torsion from Love waves as follows:

$$\ddot{\varphi}_L = \int_{-\infty}^{\infty} V_L(-i\omega) e^{i\omega t}\, d\hat{\ddot{v}}(\omega), \tag{50}$$

with $V_L = 1/(2c_L)$. From equation (50) and applying the formulae for spectral decompositions from the Appendix, the respective spectral density of torsional accelerations can be written in terms of respective translational, horizontal spectral densities as follows:

$$S_{\ddot{\varphi}L}(t,\omega) = V_L^2\omega^2 S_{\ddot{v}}(\omega). \tag{51}$$

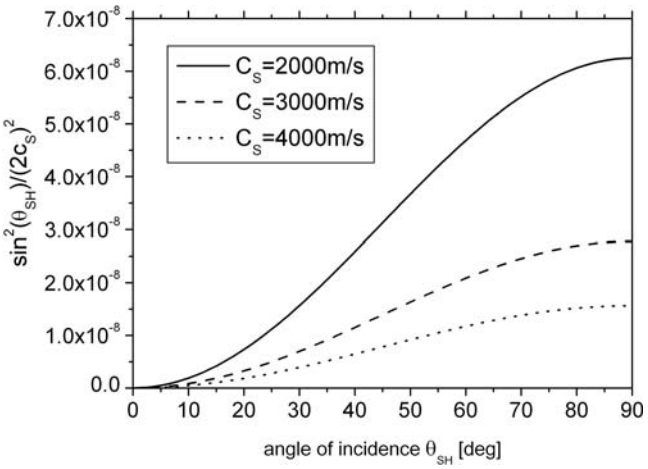

Figure 8. Coefficient $\sin^2(\Theta_{SH})/(2c_S)^2$ of equation (47) versus angle of incidence Θ_{SH}.

The question that remains to be answered regards the contribution of the *SH* waves and Love waves to the actual ground motion at a site as well as velocities of various spectral components.

Summary and Conclusions

A stochastic, analytical approach to the problem of formulating spectral densities of the rotational components of seismic ground motion from wave passage effects has been reported. After detailed analyses of body- and surface-wave decompositions at the free surface, respective formulas for rocking spectral density (around a horizontal axis), and torsional spectral density (around a vertical axis) are derived. The rotational spectral densities are formulated in terms of the translational spectral densities (horizontal and vertical) and wave parameters (propagation velocity, angle of incidence). It is interesting to note that all resulting spectral densities are functions of time derivatives of respective translational spectra (the ω^2 factor). This indicates a shift to higher frequencies of the resulting rotations in comparison to the respective translational spectral densities. It may also result in some problems when integrating the obtained spectral densities when applying the classic Kanai–Tajimi engineering spectrum, which does not decay fast enough with an increasing frequency. The article is illustrated by parametric analysis of the effect of the angle of incidence of body waves on rocking spectral density for a stiff site (firm ground) and on the effect of incidence angle of *SH* waves on the respective torsional spectral density. It is interesting to note that all these numerical analyses indicate substantial increase of the rotational ground motion with increasing angle of incidence of the body waves. As can be seen in Figure 6 these effects are particularly apparent for rocking spectral densities for overcritical angles.

To be applied in practice, the presented formulas need to include the actual (usually layered) structure of the ground beneath the site. It can be done by including the well-known Haskell–Thomson formulae (Thomson, 1950, Haskell, 1953). It should be noted that in such cases the synthesized rotational spectral densities may be quite complicated, as they would have to reflect various angles of incidence of the body waves appearing at the surface after multiple refractions and reflections; they would also have to cover various velocities of propagation of the groups of waves, including carefully chosen contributions of surface waves. One may even expect that these effects can overshadow the changes in the angle of incidence for near-field earthquakes.

However, when rotational spectral densities are finally synthesized they can easily be applied either in classic random vibration analyses of single- and multi-degree-of-freedom structural systems or to simulate rotational time histories using the Monte Carlo techniques (e.g., Rubinstein and Reuven, 2008). The detailed procedures reported in this article (after careful scaling with recorded ground motions) may serve as alternatives to other methods of generating rotational surface ground motion (e.g., Lee and Trifunac, 1985, 1987, 2009).

Data and Resources

All data used in this article came from published sources listed in the references.

References

Achenbach, J. D. (1973). *Wave Propagation in Elastic Solids*, North-Holland, Amsterdam.

Aki, K., and P. G. Richards (2002). *Quantitative Seismology*, Second Ed., University Science Books, Sausalito.

Castellani, A., and G. Boffi (1989). Rotational components of seismic motion, *Earthq. Eng. Struct. Dyn.* **18,** 785–797.

Castellani, A., and Z. Zembaty (1996). Comparison between earthquake rotation spectra obtained through different experimental sources, *Eng. Struct.* **18,** 597–603.

Flaga, A. (1979). Determining the inertia forces loading the structure implicated by ground vibrations, Papers of the Commission of Applied Mechanics, Polish Academy of Sciences, Cracow, *Mechanics* **10,** Ossilineum, 23–40 (in Polish).

Haskell, N. A. (1953). The dispersion of surface waves on multilayered media, *Bull. Seismol. Soc. Am.* **43,** 17–34.

Immamura, A. (1937). *Theoretical and Applied Seismology*, Maruzen Co., Tokyo.

Jalali, R. S., and M. D. Trifunac (2009). Response spectra for near-source, differential, and rotational strong ground motion, *Bull. Seismol. Soc. Am.* **99,** no. 2B, 1404–1415.

Lee, V. W, and M. D. Trifunac (1985). Torsional accelerograms, *Soil Dyn. Earthq. Eng.* **4,** 132–139.

Lee, V. W., and M. D. Trifunac (1987). Rocking strong earthquake accelerations, *Soil Dyn. Earthq. Eng.* **6,** 75–89.

Lee, V. W., and M. D. Trifunac (2009). Empirical scaling of rotational spectra of strong earthquake ground motion, *Bull. Seismol. Soc. Am.* **99,** no. 2B, 1378–1390.

Li, H.-N., L. E. Suarez, and M. P. Singh (1997). Rotational components of earthquake ground motions, *Earthq. Eng. Eng. Vib.* **17,** 37–50.

Li, H.-N., L.-Y. Sun, and S.-Y. Wang (2002). Frequency dispersion characteristics of phase velocities in surface wave for rotational components of seismic motion, *J. Sound Vib.* **258,** 815–827.

Newmark, N. M., and E. Rosenblueth (1971). *Fundamentals of Earthquake Engineering*, Prentice-Hall.

Niazi, M. (1986). Inferred displacements, velocities and rotations of a long rigid foundation located at El Centro differential array site during the 1979 imperial valley, California, earthquake, *Earthq. Eng. Struct. Dyn.* **14,** 531–542.

Oliveira, C. S., and B. A. Bolt (1989). Rotational components of surface strong ground motion, *Earthq. Eng. Struct. Dyn.* **18,** 517–526.

Penzien, J., and M. Watabe (1975). Characteristics of 3-dimensional earthquake ground motion, *Earthq. Eng. Struct. Dyn.* **3,** 365–373.

Richter, C. F. (1958) *Elementary Seismology*, W. H. Freeman, San Francisco.

Rubinstein, R. Y. (2008). *Simulation and the Monte Carlo Method*, John Wiley and Sons, Hoboken, New Jersey.

Rutenberg, A., and A. C. Heidebrecht (1985). Response spectra for torsion, rocking, and rigid foundations, *Earthq. Eng. Struct. Dyn.* **13,** 543–557.

Sugito, M., and K. Aizawa (1984). Simple separation technique of body and surface waves in strong motion accelerograms, *Struct. Eng./Earthq. Eng., Proc. Japan Soc. Civil Eng.*, **1**, 71–76.

Thomson, W. T. (1950). Transmission of elastic waves through a stratified solid medium, *J. Appl. Phys.* 89–93.

Trifunac, M. D. (1982). A note on rotational components of earthquake motions for incident body waves, *Soil Dyn. Earthq. Eng.* **1,** 11–19.

Trifunac, M. D. (2009). Review: rotations in structural response, *Bull. Seismol. Soc. Am.* **99,** no. 2B, 968–979.

Trifunac, M. D., and A. G. Brady (1975). On the correlation of seismic intensity scales with the peaks of recorded strong ground motion, *Bull. Seismol. Soc. Am.* **65,** 139–162.

Zembaty, Z. (1997). Vibrations of bridge structure under kinematic wave excitations, *J. Struct. Eng. ASCE* **123,** 479–488.

Zembaty, Z., A. Castellani, and G. Boffi (1993). Spectral analysis of the rotational component of earthquake motion, *Probab. Eng. Mech.* **8,** 5–14.

Appendix

Stieltjes–Fourier Representation of Stochastic Processes

The stochastic analysis of combinations of random processes standing for the ground accelerations is substantially simplified when respective processes are written in the form of Stieltjes–Fourier representation as follows.

Consider the stationary (steady) ground vibrations in the form of accelerations, for example, the seismic ground motions $\ddot{u}(t)$, $\ddot{v}(t)$, and $\ddot{w}(t)$ from Figure 1. The classic spectral representations of these three components of seismic motion treated as stationary stochastic processes take the following form:

$$\ddot{u}(t) = \int_{-\infty}^{\infty} e^{i\omega t}\, d\hat{\ddot{u}}(\omega), \qquad \ddot{v}(t) = \int_{-\infty}^{\infty} e^{i\omega t}\, d\hat{\ddot{v}}(\omega), \qquad \ddot{w}(t) = \int_{-\infty}^{\infty} e^{i\omega t}\, d\hat{\ddot{w}}(\omega), \tag{A1}$$

in which dotted symbols are random processes in the frequency domain with orthogonal increments. It means that, for example, for $\ddot{u}(t)$,

$$\langle d\ddot{u}(\omega_1) d\hat{\ddot{u}}^*(\omega_2)\rangle = \begin{cases} \langle |d\hat{\ddot{u}}(\omega)|^2\rangle = S_{\ddot{u}}(\omega)d\omega & \text{for} \quad \omega_1 = \omega_2 = \omega, \\ 0 \quad \text{for} \quad \omega_1 \neq \omega_2, \end{cases} \tag{A2}$$

where the symbol $\langle .. \rangle$ denotes mathematical expectation, an asterisk denotes complex conjugate, $S_{\ddot{u}}(\omega)$ represents power spectral density of the acceleration process $\ddot{u}(t)$, and $\omega =$ angular frequency (rad/sec). For two different processes (e.g., $\ddot{u}(t)$ and $\ddot{w}(t)$) formula (A2) takes the form

$$\langle d\ddot{u}(\omega) d\hat{\ddot{w}}^*(\omega_2)\rangle = \begin{cases} \langle |d\hat{\ddot{u}}(\omega) d\hat{\ddot{w}}^*(\omega)|\rangle = S_{\ddot{u}\,\ddot{w}}(\omega)d\omega & \text{for} \quad \omega_1 = \omega_2 = \omega, \\ 0 \quad \text{for} \quad \omega_1 \neq \omega_2, \end{cases} \tag{A3}$$

in which $S_{\ddot{u}\,\ddot{w}}(\omega)$ is the cospectral density. If the Penzien and Watabe (1975) assumption of the lack of correlation of motions among the principal axes holds, then the cospectra $S_{\ddot{u}\,\ddot{v}}(\omega)$, $S_{\ddot{u}\,\ddot{w}}(\omega)$, $S_{\ddot{w}\,\ddot{v}}(\omega)$ vanish.

Opole University of Technology
ul.Mikolajczyjka 5
45-271 Opole, Poland
z.zembaty@po.opole.pl
www.zet.po.opole.pl

Manuscript received 2 June 2008